Seven-Core Fiber Composite Structures-Based Mach-Zehnder Interferometer for Bending and Temperature Measurement

Kai ZHANG[1], Qiang LING[1,2,3*], Yao CHEN[1], Si LUO[1,4], Yusheng ZHANG[1,4], Yan ZHOU[1,4], Gaofeng FENG[2], Junyong YANG[2], Zhangwei YU[1,4], Haiyun CHEN[4], Xiuli JIANG[5], Zuguang GUAN[1,4], and Daru CHEN[1,4*]

[1]*Hangzhou Institute of Advanced Studies, Zhejiang Normal University, Hangzhou 311231, China*

[2]*Futong Group Co., Ltd., Fuyang, Hangzhou 311499, China*

[3]*College of Science, Zhejiang University of Technology, Hangzhou 310023, China*

[4]*Key Laboratory of Optical Information Detection and Display Technology of Zhejiang, Zhejiang Normal University, Jinhua 321004, China*

[5]*Department of Mathematics and Physics, University of Shanghai Electric Power, Shanghai 200090, China*

[*]Corresponding authors: Qiang LING and Daru CHEN E-mails: qianglingoptics@zjnu.edu.cn and daru@zjnu.cn

Abstract: In the paper, an optical fiber sensor based on a seven-core fiber composite structure is presented, which enables dual-parameter sensing of bending and temperature. The proposed structure is fabricated by combining the strongly-coupled seven-core fibers (SC-SCFs) and a weakly-coupled seven-core fiber (WC-SCF). The SC-SCF acts as a beam coupler and enhances the Mach-Zehnder interference, while the WC-SCF serves as the enhanced section of another Mach-Zehnder interference. Therefore, the spectrum response of the fiber structure mentioned above exhibits a superposition effect of two Mach-Zehnder interferometers (MZIs). Among them, two dips corresponding to different MZIs are used to measure bending and temperature. The experimental results show the bending sensitivity and temperature sensitivity of the two MZIs are −4.238 nm/m^{-1}, −2.263 nm/m^{-1}, 0.047 nm/℃, and 0.064 nm/℃, respectively. It proves that our sensor is very sensitive to bending. Through the dual-wavelength matrix method, the bending and temperature can be measured simultaneously. With the benefit of the composite structure, low cost, and ease of fabrication, the proposed sensor can be used in harsh environments.

Keywords: Optical fiber sensor; strongly coupled seven-core fiber; weakly-coupled seven-core fiber; bending; temperature

Citation: Kai ZHANG, Qiang LING, Yao CHEN, Si LUO, Yusheng ZHANG, Yan ZHOU, *et al*., "Seven-Core Fiber Composite Structures-Based Mach-Zehnder Interferometer for Bending and Temperature Measurement," *Photonic Sensors*, 2025, 15(1): 250131.

1. Introduction

With the advantages of compact dimensions, high sensitivity, online measurement, and long-distance transmission, optical fiber sensors are applied successively to measure temperature, bending, force, gas pressure, surrounding refractive index, and so on. Among them, bending and temperature detection are closely related to our daily life. In human motion recognition [1–4], limb bending is the key to obtaining body movements. Meanwhile, the temperature instability always

Received: 21 July 2023 / Revised: 31 January 2024

DOI: 10.1007/s13320-024-0732-2
Article type: Regular

interferes with the bending measurement. Hence, it is quite necessary to solve the problem of temperature cross-sensitivity [5, 6].

Diverse types of special optical fiber-based sensors have been proposed to realize bending and temperature measurement [7]. The special optical fiber bending sensor includes few-mode fibers (FMFs) [8], micro-structured fibers (MSFs) [9], eccentric core fibers [10], doubled-clad fiber (DCFs) [11], and multi-core fiber (MCFs) [12, 13]. Among them, MCFs are reported as a parallel type of single mode fibers (SMFs), which means an optical device to improve the data transfer capacity of SMFs. This special structure of multiple cores distributed parallelly in the cladding makes it a bright prospect to be applied in the space division multiplexing system [14]. Moreover, to suppress the inter-core crosstalk of the MCF, the weakly-coupled MCF (WC-MCF) with a large core-to-core distance is mostly utilized in information transmission [15]. Besides, the groove refractive index structure is applied to further reduce the inter-core crosstalk [16]. With the deepening of research, the applications of MCFs for the sensing field have been reported. The unique spatial structure makes it a good candidate for the measurement of bending, torsion, and other physical quantities [17, 18].

As a special MCF for sensing, the strongly coupled MCF (SC-MCF) has attracted much attention due to its high-quality output spectrum and unique super-mode characteristics [19]. For the SC-MCF, the smaller core-to-core distance results in severe crosstalk between different cores. It leads to periodic coupling among the modes in cores, which is very sensitive to the sensing parameters, such as temperature [20, 21], strain [22], force [23], refractive index [24, 25], and bending [13, 26, 27]. Especially in bending measurement, many measurement schemes have been proposed with various SC-SCF-based structures.

The Mach-Zehnder interferometer based on the strongly coupled seven-core fiber (SC-SCF) has been investigated for bending sense [23]. The bending sensitivity of the MZI sensor based on a 4.5 cm-SC-SCF is 2.65 nm/m^{-1} with an insertion loss of −2 dB. Compared with the MZI bending sensor based on the weakly coupled seven-core fiber (WC-SCF) with the bending sensitivity of −15.567 nm/m^{-1} [28], the sensitivity of the SC-SCF is noticeably slightly lower. Due to the size of the central core of the WC-SCF, which is quite close to that of the SMF, it is necessary to utilize a multi-mode fiber (MMF) to expand the beam. However, the MMF not only increases the size of the sensor but also brings an insertion loss of −15dB, which limits its application. As an optical thermometer, SC-MCFs can withstand the high temperature environment up to 1 000 ℃ and exhibit the temperature sensitivity of about 50 pm/℃ [20, 28]. Therefore, it is necessary to achieve simultaneous detection, which limits its application. For this purpose, the super-mode Bragg grating inscribed in the SC-SCF has been used for temperature and bending simultaneous measurement [26]. In the design, the resonant peaks and dips of the interference spectrum for the SC-SCF-based MZI show different responses to bending and temperature. The maximum resolutions due to bending and temperature for the two wavelengths are −112.3 pm/m^{-1}, 9.55 pm/℃, 3.909 nm/m^{-1}, and 11.8 pm/℃, respectively.

In this paper, to measure the bending and temperature simultaneously, a composed sensor is proposed, fabricated by the fusion splicing WC-SCF between two short pieces of SC-SCFs. The two SC-SCFs act as the beam couplers and MZI-enhanced sections. The WC-SCF is introduced to enhance another Mach-Zehnder interference. Due to two types of SCFs, their spectra are superimposed. Therefore, based on the dual wavelength matrix demodulation method, the simultaneous measurement of bending and temperature can be achieved. The advantages of our sensors are clear. Using low-cost materials, sensors

can be made to measure both bending and temperature.

2. Structure and sensing principles

The schematic diagram of the composite structure-based MZI is shown in Fig. 1(a). It consists of the lead-in/lead-out SMF, two sections of SC-SCFs, and a section of the WC-SCF. The structure is fabricated by successively splicing the three types of optical fibers through the fusion splicer (Fujikura, 80S, Japan). The lengths of the SC-SCF and WC-SCF are L_1 and L_2, respectively. When cutting optical fibers, the cutting position and the distance from the coating stripping point to the cutting point can be controlled by adjusting the position of the fiber relative to the scales. The WC-SCF, provided by Yangtze Optical Fiber Company, China, has the cross-section image as shown in Fig. 1(b). The diameters of the outer cladding and cores are 150 μm and 8 μm, respectively, with a distance between two neighboring cores of 41.5 μm. The refractive index difference between the core and cladding is 0.004 9. Figure 1(c) gives the micrograph of the SC-SCF, which is homemade by the stack-and-draw technique [27]. The diameters of the outer cladding and cores are 125 μm and 8.2 μm, respectively with a distance between adjacent cores of 11 μm. The refractive index difference between the core and cladding is 0.004 9. The SMF from Corning, USA has a core diameter of 8.5 μm and a cladding diameter of 125 μm.

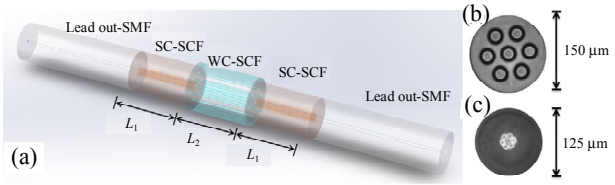

Fig. 1 Sensors for bending and temperature detection: (a) schematic diagram of the proposed MZI-based sensor, and the cross-section view of the (b) WC-SCF and (c) SC-SCF.

The optical field distribution of the proposed MZI-based structure is shown in Fig. 2, which is numerically simulated by RSoft. The simulation results show that when the light injects from the core of the lead-in SMF into the core of the SC-SCF, the light splits into the central core and the other six cores. When the light reaches the first fusion point between the SC-SCF and the WC-SCF, some energy is split to the higher-order mode of the WC-SCF rather than the other six cores of the WC-SCF, because the six cores of the WC-SCF are too far from the central core. Residual energy is coupled to the center of the WC-SCF. Afterwards, the light injects from the WC-SCF into the second SC-SCF, which enhances the MZI and also acts as a beam coupler, coupling the energy of the higher order mode in the WC-SCF back into the lead-out SMF. The proposed structure contains three MZIs. One corresponds to the super modes of the SC-SCF, and the others occur between the fundamental mode and higher-order modes of the WC-SCF.

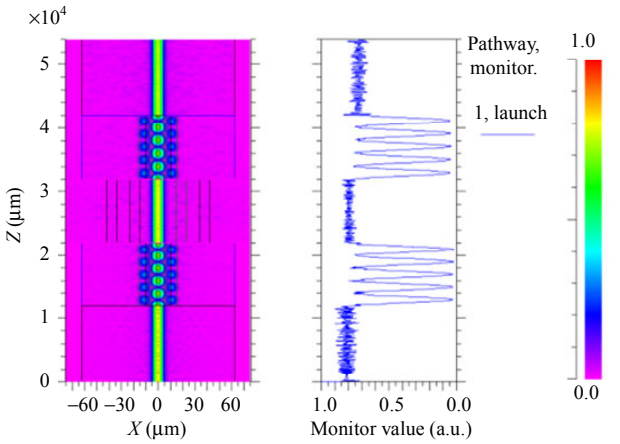

Fig. 2 Light field distribution of the SCFs composite structure (L_1=10 mm and L_2=10 mm).

Figure 3 shows the experimental results of the transmission spectrum and the spatial spectrum for the proposed sensor. The maximum fringe visibility near 1 356 nm reaches 24 dB, while the insert loss is only about 2.9 dB. Compared with the measured transmission spectra of the SC-SCF-based MZI and the WC-SCF-based MZI as illustrated in Fig. 4, its insert loss is close to that of the SC-SCF, and it has a stronger interference effect than the WC-SCF. Moreover, the illustrated MZI spectra designed by us exhibit the effect of multi-interference

superposition, which can be observed in the inset of Fig. 3. The highest dominant peak appears at 0.007 5 nm^{-1}, corresponding to the free spectral range of 133.33 nm, which is caused by the interference between the two super modes of the SC-SCF at the wavelength of 1 359 nm (Dip 1). The second dominant peak appears at 0.025 nm^{-1} and is caused by the interference between the fundamental core mode and the higher mode of the WC-SCF at the wavelength of 1 390 nm (Dip 2). The effective refractive indexes of the fundamental core mode and the first-order core mode excited in the SC-SCF are 1.442 5 and 1.441 8 at the wavelength of 1 390 nm. It can be determined that the highest peak at 0.007 5 nm^{-1} is caused by the interference between the two super modes of the SC-SCF at the wavelength of 1 390 nm. Similarly, the effective refractive indexes of the fundamental core modes of the central core and outer six cores for the WC-SCF are 1.442 072 929 and 1.437 860 359, respectively. It can be determined that the highest peak at 0.025 nm^{-1} is caused by the interference between the two super modes of the SC-SCF at the wavelength of 1 359 nm. The two SCFs play different roles in the composited sensor. The advantages of the SC-SCF are the low insertion because of the mode filed characteristics of super modes, and the WC-SCF in our sensor proves the ability of high response to curvature changes.

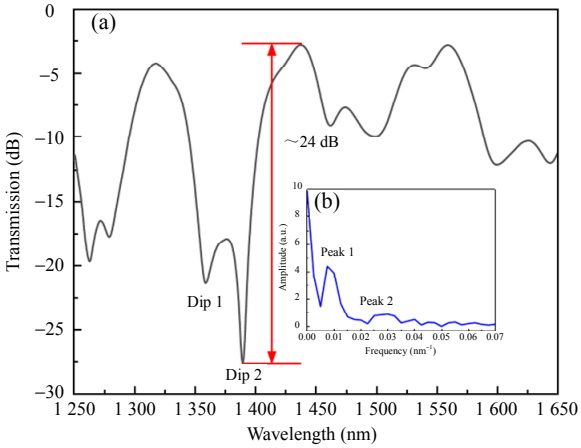

Fig. 3 Spectral analysis: (a) measured transmission spectra and (b) spatial frequency spectra.

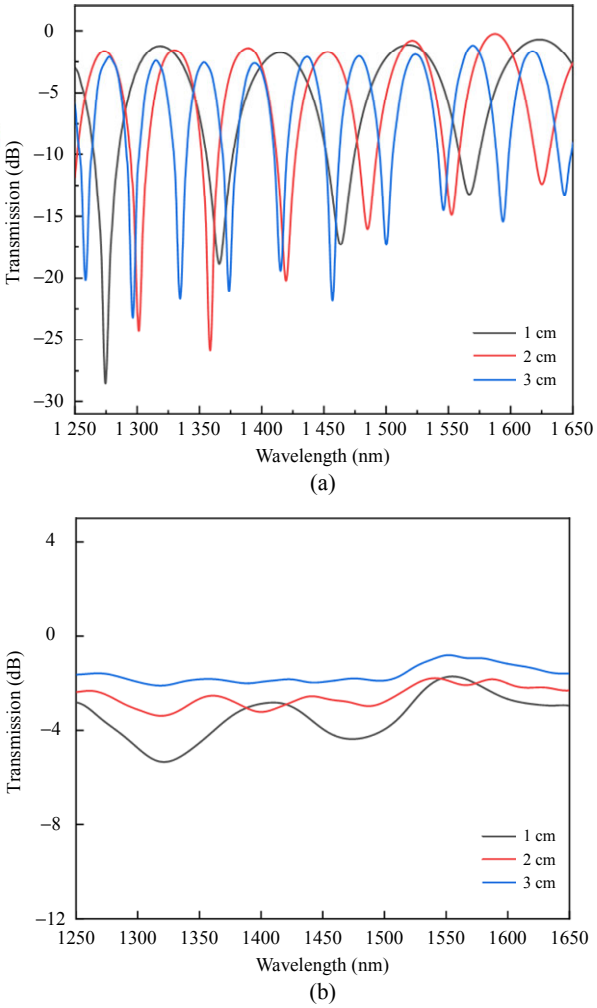

Fig. 4 Measured transmission spectra of the (a) SC-SCF-based MZI and (b) WS-SCF-based MZI.

3. Experimental results and discussion

The bending and temperature responses of the proposed sensor have been experimentally studied, as shown in Fig. 5. The setup consists of a super luminescent diode (SLD, Denselight, China), an optical spectrum analyzer (OSA, Yokogawa Electric Corporation, AQ6375, Japan), two 3-axis roller block stage (Thorlabs, RBL13D, USA), and a thermostat. The light with a broadband of 1 250 nm–1 650 nm from the SLD transmits into the sensor, and then the filtered spectra are received by the OSA with a resolution of 0.05 nm.

In the bending measurement, when the bending changes, the temperature is kept at room temperature of 26 ℃. The lead-in SMF and lead-out SMF are

fixed on the two 4-axis translation stages, respectively. By adjusting the distance between the two stages, the bending can be adjusted, as shown as [28]

$$C \approx \sqrt{24d/L^3} \quad (1)$$

where d is the distance difference between the two translation stages and increases from 0 mm to 0.4 mm with an increment interval of 0.05 mm. L is the distance between the two stages, which is set as 11.46 cm.

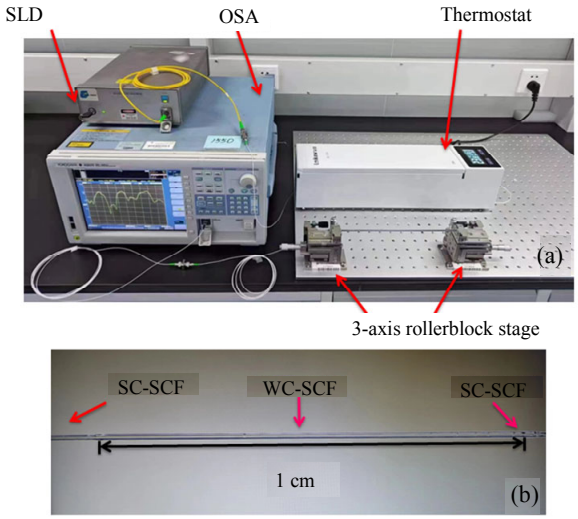

Fig. 5 Experimental setup of the bending and temperature measurement.

Figures 6(a) and 6(b) show the transmission spectra under different bending for the sensor with L_1=1.0 cm and L_2=1.0 cm in the bending ranges from 0 m^{-1} to 2.6494 m^{-1}. It shows that the interference dips have a significant blue shift, which is consistent with the reported results [27, 28]. For bending sensing, the interference wavelength is mainly affected by the strain-induced refractive index changes. In the process of the curvature increasing, there is a negative correlation between the wavelength shift and the strain-induced refractive index coefficient [29]. Thus, the blue shift in the bending increasing process is reasonable.

After repeated measurements three times, the wavelengths versus bending for Dips 1 and 2 are shown in Fig. 6(c). It is obvious that Dip 1 has the higher bending sensitivity than Dip 2. The two dips in three measurements illustrate a good linear response. In the range from 0 m^{-1} to 0.9367 m^{-1}, the sensor is affected not only by the curvature, but also by the prestress. The maximum standard deviation in the whole cycle for the two dips are 0.46 nm and 0.17 nm, respectively. It proves the good reliability of the proposed sensor. According to the experimental results, the sensitivity of the two dips in the range of 0.9367 m^{-1}–2.6494 m^{-1} is −4.238 nm/m^{-1} and −2.263 nm/m^{-1}, respectively, with a linear fit with high adj. R^2 of 0.989 and 0.992.

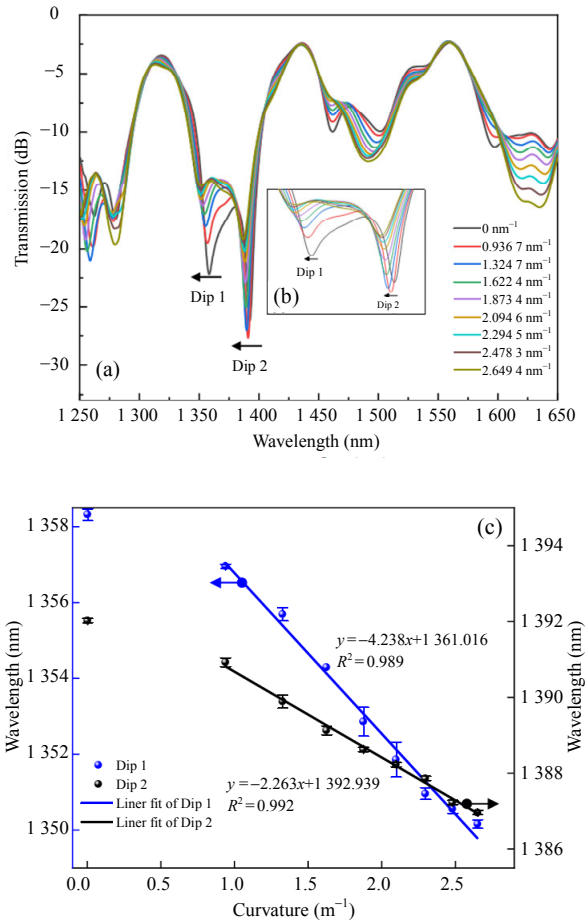

Fig. 6 Bending measurement: (a) transmission spectra under different bending, (b) detail view, and (c) relationship between the bending and dip wavelengths for Peaks 1 and 2.

For the temperature sensing, the sensor is placed on the thermostat, as shown in Fig. 5. The ambient temperature increases from 30 ℃ to 80 ℃ with a step of 5 ℃. At each test, the temperature is kept for 5 min to ensure the temperature stability. Figure 7 shows the transmission spectra under different

temperatures, which are repeated 3 times. All dips have an obvious red shift when the temperature increases. The linear fitting curve shows that the two dips have good linearity with high adj. R^2 of 0.997 and 0.990, and the sensitivity of 0.047 nm/℃ and 0.064 nm/℃, respectively. For three times measurements, the maximum standard deviation for the two dips are 0.150 nm and 0.058 nm, respectively. This proves the good repeatability of the proposed sensor. Meantime, based on the different spectrum responses for bending and temperature of different MZIs, a dual wavelength matrix can be built to measure the two environmental parameters simultaneously.

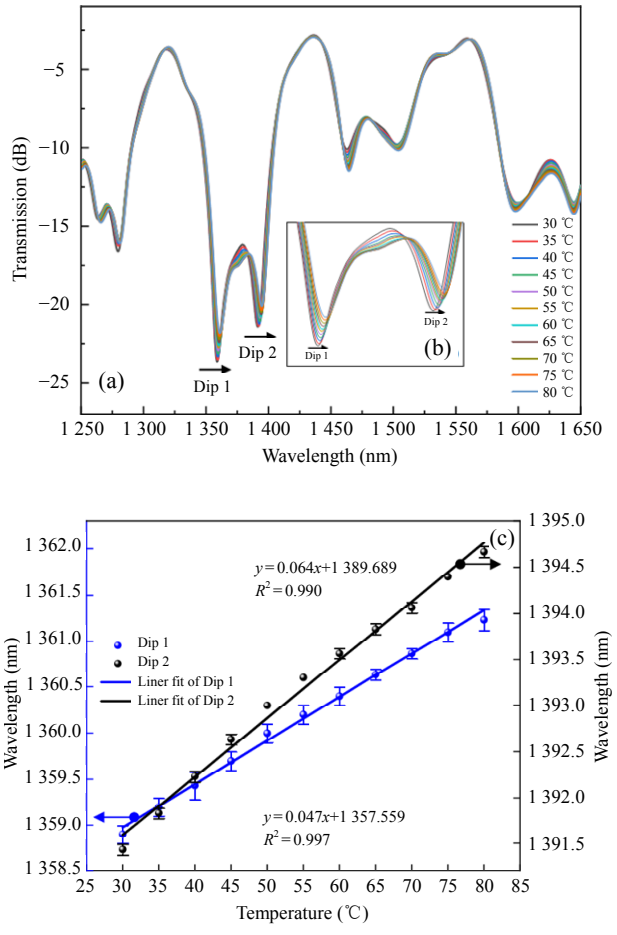

Fig. 7 Temperature measurement: (a) transmission spectra under different temperatures, (b) detail view, and (c) relationship between the temperature and dip wavelengths.

For the proposed sensor, the wavelengths shift under different bending and temperatures can be expressed as

$$\Delta\lambda_{\text{Dip 1}} = K_{11}\Delta C + K_{12}\Delta T \tag{2}$$

$$\Delta\lambda_{\text{Dip 2}} = K_{21}\Delta C + K_{22}\Delta T \tag{3}$$

where K_{11}, K_{12}, K_{21}, and K_{22} are the bending sensitivity and the temperature sensitivity of two dips, respectively. These have been calculated in the above state. Based on the dual-wavelength matrix method, the relationship between the wavelengths and the two environmental parameters can be expressed as

$$\begin{bmatrix}\Delta\lambda_{\text{Dip 1}}\\ \Delta\lambda_{\text{Dip 2}}\end{bmatrix} = \begin{bmatrix}K_{11} & K_{12}\\ K_{21} & K_{22}\end{bmatrix}\begin{bmatrix}\Delta C\\ \Delta T\end{bmatrix}. \tag{4}$$

When the unknown bending and temperature are applied to the sensor, the bending and temperature can be demodulated as

$$\begin{bmatrix}\Delta C\\ \Delta T\end{bmatrix} = \begin{bmatrix}K_{11} & K_{12}\\ K_{21} & K_{22}\end{bmatrix}^{-1}\begin{bmatrix}\Delta\lambda_{\text{Dip 1}}\\ \Delta\lambda_{\text{Dip 2}}\end{bmatrix}. \tag{5}$$

Substituting the sensitivity in the experiments, the bending and temperature can be calculated as

$$\begin{bmatrix}\Delta C\\ \Delta T\end{bmatrix} = \begin{bmatrix}-4.238\,\text{nm/m}^{-1} & 0.047\,\text{nm/℃}\\ -2.263\,\text{nm/m}^{-1} & 0.064\,\text{nm/℃}\end{bmatrix}^{-1}\begin{bmatrix}\Delta\lambda_{\text{Dip 1}}\\ \Delta\lambda_{\text{Dip 2}}\end{bmatrix}. \tag{6}$$

Table 1 compares the bending sensitivity and temperature sensitivity of the sensor in our work with the previous publications. Compared with the optical fiber grating-based bending sensors, the sensitivity of our sensor reaches the average level with the simpler fabrication method and lower cost. The typical MZI sensors have higher bending sensitivity and can achieve simultaneous measurement of two parameters.

4. Conclusions

In summary, the composed sensor based on the SC-SCF-WC-SCF-SC-SCF with the ability of dual-parameter sensing is presented and demonstrated experimentally. The dual-type SCFs splicing structure excites two MZIs. By utilizing the different sensitivity of MZIs to bending and temperature responses, it is easy to achieve dual parameter demodulation. The experimental results show the maximum bending sensitivity reaches 4.238 nm/m^{-1} in the range of 0.936 7 m^{-1}–

2.649 4 m^{-1}, and the maximum temperature sensitivity is 0.064 nm/℃ in the range of 30 ℃–80 ℃. With the advantages of the simple structure, easy fabrication, high sensitivity, and dual-parameter measurement, the proposed sensor is more suitable in various fields, such as the environment, bridges, dams, oil fields, clinical medical inspection, and food safety inspection.

Table 1 Comparison of the typical bending sensor.

Configuration	Bending sensitivity (nm/m^{-1})	Range (m^{-1})	Temperature sensitivity (pm/℃)	Fabricated method	Two-parameter	Ref.
SC-SCF-based FBG	−3.909 8	0–0.494 0	11.80	FBG fabricated by 193 nm excimer laser	Yes	[26]
Two non-orthogonal LPFG	3.234	0–0.588 0	56.00	LPFG fabricated by CO_2 laser	Yes	[12]
SPR based on D-type double-clad multimode fiber	0.611 4	0–45.977 0	-	-	No	[11]
FMF-based MZI	2.00	0–10.000 0	10.65	MZI enhanced by CO_2 laser	No	[8]
SCF-based composed MZIs	4.238	0.936 7–2.649 4	64.00	Fusion splicing	Yes	Our work

Acknowledgment

This work is supported by “Pioneer” and “Leading Goose” Research & Development Program of Zhejiang, China (Grant No. 2022C03084), the Natural Science Foundation of China (Grant No. 62205296), the Zhejiang Provincial Natural Science Foundation of China (Grant Nos. LQ22F050007 and LQ23F050004), and the Ningbo Science and Technology Project, China (Grant No. 2021Z030).

Declarations

Conflict of Interest The authors declare that they have no competing interests.

Permissions All the included figures, tables, or text passages that have already been published elsewhere have obtained the permission from the copyright owner(s) for both the print and online format.

References

[1] S. Q. Liu, J. C. Zhang, Y. Z. Zhang, and R. Zhu, “A wearable motion capture device able to detect dynamic motion of human limbs,” *Nature Communications*, 2020, 11(1): 5615.

[2] B. Yin, Y. Li, Z. B. Liu, S. Feng, Y. Bai, Y. Xu, *et al*., Investigation on a compact in-line multimode-single-mode-multimode fiber structure,” *Optics & Laser Technology*, 2016, 80: 16–21.

[3] C. Guan, X. Zhong, G. Mao, T. Yuan, J. Yang, and L. Yuan, “In-line Mach-Zehnder interferometric sensor based on a linear five-core fiber,” *IEEE Photonics Technology Letters*, 2015, 27(6): 635–638.

[4] L. Duan, P. Zhang, M. Tang, R. Wang, Z. Zhao, S. Fu, *et al*., “Heterogeneous all-solid multicore fiber based multipath Michelson interferometer for high temperature sensing,” *Optics Express*, 2016, 24(18): 20210–20218.

[5] S. Zhou, B. Huang, and X. Shu, “A multi-core fiber based interferometer for high temperature sensing,” *Measurement Science and Technology*, 2017, 28(4): 045107.

[6] W. Yuan, Q. Zhao, L. Li, Y. Wang, and C. Yu, “Simultaneous measurement of temperature and curvature using ring-core fiber-based Mach-Zehnder interferometer,” *Optics Express*, 2021, 29(12): 17915–17925.

[7] Q. Wang and Y. Liu, “Review of optical fiber bending/curvature sensor,” *Measurement*, 2018, 130: 161–176.

[8] R. Zhao and X. W. Shu, “Curvature sensor based on femtosecond laser-inscribed straight waveguide in FMF,” *Optics & Laser Technology*, 2022, 152: 108154.

[9] D. Pereira, J. Bierlich, J. Kobelke, and M. S. Ferreira, “Simultaneous measurement of strain, curvature, and temperature using a hollow square core fiber,” *Optics and Laser Technology*, 2022, 156: 108540.

[10] L. Ding, J. Li, Y. Deng, S. Xiao, J. Wang, and Y. Tian, “An inline fiber curvature sensor based on eccentric

core fiber and off-axis air cavity Fabry-Pérot interferometer," *IEEE Sensors Journal*, 2019, 19(19): 8700–8705.

[11] Y. Wei, C. Liu, C. Liu, C. Shi, Z. Ren, Z. Ran, *et al*., "Multichannel directional recognition SPR curvature sensor based on D-type double-clad multimode fiber," *IEEE Sensors Journal*, 2022, 22(22): 21719–21726.

[12] S. Wang, W. Zhang, L. Chen, Y. Zhang, P. Geng, Y. Zhang, *et al*., "Two-dimensional microbend sensor based on long-period fiber gratings in an isosceles triangle arrangement three-core fiber," *Optics Letters*, 2017, 42(23): 4938–4941.

[13] Z. Liu, D. Zheng, J. Madrigal, J. Villatoro, J. E. Antonio-Lopez, A. Schülzgen, *et al*., "Temperature-insensitive curvature sensor based on Bragg gratings written in strongly coupled multicore fiber," *Optics Letters*, 2021, 46(16): 3933–3936.

[14] C. Caucheteur, J. Villatoro, F. Liu, M. Loyez, T. Guo, and J. Albert, "Mode-division and spatial-division optical fiber sensors," *Advances in Optics and Photonics*, 2022, 14(1): 1–86.

[15] L. Sun, J. Zhang, G. Zhou, B. Chen, G. N. Liu, Y. Cai, *et al*., "Theoretical investigations of weakly- and strongly-coupled multi-core fibers for the applications of optical submarine communications under power and fiber count limits," *Optics Express*, 2023, 31(3): 4615–4629.

[16] C. Wang, S. Li, X. Li, Z. Li, P. Shao, Y. Guo, *et al*., "Trench-assisted 12-core 5-LP mode fiber with a low refractive index circle and a high refractive index ring," *Optics Express*, 2023, 31(5): 7290–7302.

[17] J. B. Wang, X. Z. Zeng, J. Zhou, J. Y. Hao, X. Yang, Y. Liu, *et al*., "Highly sensitive torsion sensor based on Mach-Zehnder interference in helical seven-core fiber taper," *Chinese Optics Letters*, 2023, 21(4): 041205.

[18] D. Paloschi, K. A. Bronnikov, S. Korganbayev, A. A. Wolf, A. Dostovalov, and P. Saccomandi, "3D shape sensing with multicore optical fibers: transformation matrices versus Frenet-Serret equations for real-time application," *IEEE Sensors Journal*, 2020, 21(4): 4599–4609.

[19] Y. C. Yao, Z. Y. Zhao, and M. Tang, "Advances in multicore fiber interferometric sensors," *Sensors*, 2023, 23(7): 3436.

[20] J. E. Antonio-Lopez, Z. S. Eznaveh, P. LiKamWa, A. Schülzgen, and R. Amezcua-Correa, "Multicore fiber sensor for high-temperature applications up to 1 000 ℃," *Optics Letters*, 2014, 39(15): 4309–4312.

[21] J. Amorebieta, A. Ortega-Gomez, R. Fernández, E. Antonio-Lopez, A. Schülzgen, J. Zubia, *et al*., "Sensitivity-optimized strongly coupled multicore fiber-based thermometer," *Optics & Laser Technology*, 2022, 145: 107532.

[22] J. Villatoro, O. Arrizabalaga, G. Durana, I. Sáez de Ocáriz, E. Antonio-Lopez, J. Zubia, *et al*., "Accurate strain sensing based on super-mode interference in strongly coupled multi-core optical fibres," *Scientific Reports*, 2017, 7(1): 4451.

[23] A. Van Newkirk, J. E. Antonio-Lopez, G. Salceda-Delgado, M. U. Piracha, R. Amezcua-Correa, and A. Schülzgen, "Multicore fiber sensors for simultaneous measurement of force and temperature," *IEEE Photonics Technology Letters*, 2015, 27(14): 1523–1526.

[24] J. A. Flores-Bravo, R. Fernández, E. A. Lopez, J. Zubia, A. Schülzgen, R. A. Correa, *et al*., "Simultaneous sensing of refractive index and temperature with a supermode interferometer," *Journal of Lightwave Technology*, 2021, 39(22): 7351–7357.

[25] Y. H. Xie, C. Wu, J. Li, and B. O. Guan, "Thinned multicore fiber supermode Bragg grating and interferometer for temperature-compensated refractive index sensing," *Journal of Lightwave Technology*, 2023, 41(13): 4473–4480.

[26] X. Dong, Y. H. Xie, J. L. Ou, C. Wu, J. Li, and B. O. Guan, "Supermode Bragg grating inscribed in a strongly coupled seven-core fiber and its responses to temperature and curvature," *Optics Express*, 2023, 31(2): 3258–3268.

[27] Y. Zhou, Y. Wang, H. B. Liu, J. Chen, P. Yang, L. She, *et al*., "High-sensitive bending sensor based on a seven-core fiber," *Optics Communications*, 2021, 483: 126617.

[28] Q. Wang and Y. Liu, "Optical fiber curvature sensor based on MMF-SCF-MMF structure," *Optical Fiber Technology*, 2018, 43: 1–5.

[29] X. J. Zhu, Y. Q. Pan, A. Sun, D. Sun, W. Liu, J. Cao, *et al*., "High sensitivity curvature sensor based on a double-sphere tapered no-core fiber Mach-Zehnder interferometer," *Optics and Laser Technology*, 2022, 155: 108364.